frontiers | Frontiers in Mechanical Engineering

TYPE Original Research
PUBLISHED 24 April 2024
DOI 10.3389/fmech.2024.1393088

OPEN ACCESS

EDITED BY
Abdelmageed A. Elmustafa,
Old Dominion University, United States

REVIEWED BY
Chitaranjan Pany,
Vikram Sarabhai Space Centre, India
Davood Rahmatabadi,
University of Tehran, Iran

*CORRESPONDENCE
Sivaprakasam Palani,
shiva_au@rediffmail.com

RECEIVED 28 February 2024
ACCEPTED 08 April 2024
PUBLISHED 24 April 2024

CITATION
Gebreamlak G, Palani S, Sirahbizu B and Čep R (2024), Experimental investigation and optimization of nano Al_2O_3 mixed FSWed joint between AA2024-T351 and AA7075-T651 by response surface approach.
Front. Mech. Eng 10:1393088.
doi: 10.3389/fmech.2024.1393088

Experimental investigation and optimization of nano Al_2O_3 mixed FSWed joint between AA2024-T351 and AA7075-T651 by response surface approach

Getachew Gebreamlak[1], Sivaprakasam Palani[1]*, Belete Sirahbizu[1] and Robert Čep[2]

[1]Department of Mechanical Engineering, College of Engineering, Nano Technology (CoE), Addis Ababa Science and Technology University, Addis Ababa, Ethiopia, [2]Department of Machining, Faculty of Mechanical Engineering, VSB-Technical University of Ostrava, Ostrava, Czechia

Additive mixed friction stir welding can be an innovative and novel method for enhancing the friction stir welding process. Thus, this research aimed to investigate nano Al_2O_3 effects on the mechanical and microstructure of FSWed joints using Al alloys AA2024-T351/AA7075-T651. The experiments were performed based on response surface approach based CCD twenty run with varying three factors: tool rotational speed (A: 800–1,200 rpm), welding speed (B: 20–60 mm/min), tool plunge depth (C: 0.2–0.4 mm) and fixed volume percentages of Al_2O_3 nano-particles (8%). Mechanical performances such as tensile, yield, and hardness tests have been performed and microstructural properties have been analyzed through SEM and microscopy. The statistical analysis shows that the tensile strength can be significantly affected by rotational speed (A), welding speed (B), tool plunge depth (C), interaction (AB, BC, AC), and quadratic term A^2, B^2 in the FSW process; yield strength was influenced considerably by main, interaction, and quadratic terms; main factors and quadratic terms A^2, B^2 and C^2 significantly influenced hardness values. The fracture test revealed that the joints with Al_2O_3-reinforced AA2024-T351/AA7075-T651 alloys were more ductile and less brittle. The optimal conditions for FSW, tool rotational at 1,146 rpm, weld speed at 60 mm/min, and 0.4 mm plunge depth were responsible for higher tensile strength of 169 MPa, yield strength of 145 MPa, and micro-hardness values of 89 HRB due to the uniform nano-particle dispersions and better material mixing.

KEYWORDS

nano-particles, tensile strength, micro-hardness, friction stir welding, Al_2O_3

1 Introduction

Many industrial applications have found it advantageous to join distinct materials to attain the required mechanical and microstructural properties and increase production outputs. Most of the structures in the aerospace and automotive industries are constructed from dissimilar metals and alloys to meet the demand for lightweight and structural performance. However, joining these dissimilar metals and creating a successful welded joint between them is always challenging because different metals have distinct qualities, both chemical and physical. The

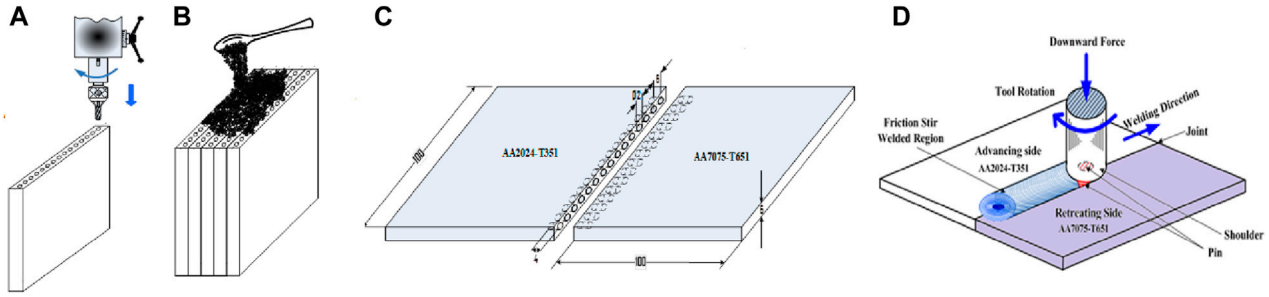

FIGURE 1
Schematic diagram **(A)** Drilling holes on the edge of the plate **(B)** Al_2O_3 nanoparticle addition **(C)** Butt position of the material and **(D)** FSW Process.

production of high residual stresses and brittle intermetallic compounds (IMCs) makes welding dissimilar metals difficult (Gebreamlak G et al., 2022). The main problem with the traditional fusion welding procedure is the filler material's miscibility with the base materials (Sahu, S., et al., 2021). The growth of IMCs and lack of mixing were caused by differences in the physical properties of the base materials, such as their melting temperature and thermal expansion coefficient. The solution to the welding problems of residual stress and IMCs between different metals was reviewed by Fang Y. et al. (2019). In various welding processes, employing intermediate interlayers can prevent or reduce the production of brittle intermetallic reaction layers.

Adding nanoparticle reinforcement to the metal matrix will further improve the weld properties of FSW joints. Nano-sized material-reinforced FSW is a newly emerging technology for enhancing the properties of welded joints through composite joints. The dispersion of grain particles in the heat-affected zone (HAZ) was limited, and the microstructure of the WNZ was refined with addition of the Al_2O_3 nanoparticle to the Al alloy. The zener pinning effect generated by the nano alumina particles, which inhibit grain expansion by recrystallization, was the source of the extraordinary refinement of grains in the WZA. Adding nanoparticles in the WNZ significantly increased the sample's wear resistance, tensile strength, and hardness than the normal FSW. The specimen unexpectedly fractured under tensile stress because single pass FSW caused an uneven dispersion of Al_2O_3 nanoparticles. This led to void initiation at the HAZ's boundary between the Al alloy and nano alumina (Singh, T et al., 2019).

FSW process parameters significantly affect the dispersion of reinforcing nanoparticles, which enhances the welded joint properties through grain refinement (Vimalraj and Kah, 2021). Morales et al. (2022) studied the effects of adding Al_2O_3-SiC reinforcing particles on the mechanical and microstructural characteristics of FSWed joints made of distinct Al alloys 2024 and 7,075. The resulting joint of the FSW of dissimilar metals became promising for demanding applications of industrial sectors for excellent mechanical and micro-structural properties. Jain and Mishra, (2022a) studied the impact of Al_2O_3 with varying volume fractions in FSW factors between AA7075/AA6061. The investigation found that the dispersion of Al_2O_3 nanoparticles significantly influences the enhancement of mechanical characteristics, the resulting pinning mechanism, and the dynamic recrystallization within the WNZ.

The reinforcing with 0, 5, 8, and 13% (vol% fraction) of $SiCN_P$ into grooves with widths of 0, 0.2, 0.3, and 0.5 mm composite joints were produced at the WNZ. At 5 vol% fraction of FSW joint specimen for double pass processing exhibited increased elongation %, yield, and tensile strength and a homogenous, defect-free dispersal of $SiCN_P$ with an average grain size of roughly 2–3 μm at the WNZ (Kumar, K. et al., 2019). The deformation behavior during welding and frictional heating might be affected by including ceramic particles in the welded plates. As a result, there may be changes to the welds' mechanical properties and microstructure (Mirjavadi, S.S et al., 2017; Moustafa, E., 2017). Empirical research has demonstrated that adding ceramic particles to the plates that are FSWed joints enhance the tensile strength (Abnar, B. et al., 2023; Kundu, A.K. et al., 2022).

The strength and rigidity of the composite are determined mainly by the grain size and particle distribution that reinforce inside the matrix (He T. et al., 2019; Hassan A. et al., 2023).

However, FSW has become a noticeable improvement in nanocomposites' tensile strength in recent years. The mechanical characteristics of MMCs made of fly ash and SiC-reinforced AA2024 alloy were investigated (Boopathi M. et al., 2013). The results showed a favorable relationship between the composite material's toughness, tensile strength, and the tool's rotating velocity. 10 vol% Al_2O_3-reinforced 7,005 aluminum alloys and 20 vol% Al_2O_3-reinforced 6,061 aluminum alloys were examined for their tensile and low-cycle fatigue performance. The results show that the composite material's toughness and tensile strength were positively correlated with the tool's rotation speed (Ceschini, L et al., 2006).

Critical strains occurred across the weld zone and caused rupture due to laser heat and metallurgical changes in the base metal during pre-softening (Aminzadeh et al., 2021). The sample with the maximum tensile strength of 208.13 MPa was made using a square pin, 1,200 rpm rotational speed, and 120 mm/min welding speed. Welding speeds have a beneficial impact on micro-hardness, resulting in greater values compared to rotating speeds. RSM was successfully used, with *p*-values below 0.05 indicating significant fitted models (Ahmadi M et al., 2022). The empirical relations employed to evaluate the burst pressure from Young's modulus, yield strength, and tensile strength of the material (Pany et al., 2012; Pany, 2021b). It is too costly, time-consuming, or difficult to eliminate the causes of this quality degradation. A robust design process is an alternative way to reduce this divergence (Vamsi A. et al., 2021). An inverse Ramberg-Osgood equation illustrates the material's stress-strain curve (Pany, 2021a). A power law model of crack growth as a function of the stress intensity factor is used to calculate the

TABLE 1 FSW factors and various level.

Symbol	Factors	Levels				
		-α	Low	Middle	High	+α
A	Rotational Speed (rpm)	663.64	800	1,000	1,200	1,336.4
B	Welding Speed (mm/min)	6.36	20	40	60	73.64
C	Plunge Depth (mm)	0.13	0.2	0.3	0.4	0.47

TABLE 2 RSM- CCD and experimental results of FSW.

Run order	Rotational speed	Welding speed	Plunge depth	Tensile strength (TS)	Yield strength (YS)	Micro-hardness
	rpm	mm/min	mm	MPa	MPa	HRB
1	800.00	60.00	0.20	127.47	122.532	86.7
2	1,200.00	60.00	0.20	131.22	127.03	86.5
3	1,000.00	40.00	0.30	149.06	142.65	88.2
4	1,000.00	40.00	0.30	148.07	142.66	88.5
5	1,000.00	40.00	0.47	151.21	135.599	87.93
6	1,000.00	40.00	0.30	149.01	142.09	88.4
7	1,200.00	60.00	0.40	170	143	89
8	800.00	60.00	0.40	132.92	122.94	87.39
9	800.00	20.00	0.20	144.02	136.843	80.4
10	1,000.00	40.00	0.30	149.99	142.86	88.7
11	800.00	20.00	0.40	126.56	120.603	82.92
12	1,200.00	20.00	0.20	130.28	123.02	81.61
13	663.64	40.00	0.30	119.2	116.89	84.5
14	1,000.00	73.64	0.30	139.72	130.381	85.53
15	1,200.00	20.00	0.40	134.61	120.77	82.77
16	1,000.00	6.36	0.30	135.11	125	77.1
17	1,000.00	40.00	0.13	139.29	137.071	86.3
18	1,336.36	40.00	0.30	127.03	121.05	84.9
19	1,000.00	40.00	0.30	150.19	142.5	88.45
20	1,000.00	40.00	0.30	149.66	142.33	88

maximum failure load of weld samples (Sundaresan and Nageswara Rao, 2014).

In FSW, including nanoparticles in the Al matrix and their impact on mechanical and microstructural properties has been the subject of much recent research. However, the FSW of Al alloys AA2024-T351 and AA7075-T651 with nano Al_2O_3 enhancement has yet to be examined. Applying nano Al_2O_3 particle reinforcement to various aluminum alloys via FSW can be innovative. Thus, this research aimed to investigate nano Al_2O_3 effects on the mechanical and microstructure of FSWed joints. This paper investigates the effects of FSW factors on the Tensile Strength (TS), Yield Strength (YS), and Microhardness (MH) of FSWed joints made between dissimilar grades of aluminum alloys, 2024-T351 and 7075-T651. The mathematical model was developed for the prediction of responses. The desirability approach was used for optimization to find the optimal FSW conditions of aluminum alloy.

2 FSW materials and process

2.1 FS weld and tool materials

The aluminum alloy square plates (100 mm × 100 mm, 6 mm thick) with the designations AA2024-T351 and AA7075-T651

TABLE 3 ANOVA table for tensile strength (MPa).

Source	*SS	**df	***MS	F-value	*p*-value Prob > F	
Model	2,699.11	8	337.39	45.97	<0.0001	Significant
A-Rotational speed	170.87	1	170.87	23.28	0.0005	
B-Welding speed	84.11	1	84.11	11.46	0.0061	
C-Plunge Depth	191.55	1	191.55	26.10	0.0003	
AB	270.53	1	270.53	36.86	<0.0001	
AC	379.79	1	379.79	51.75	<0.0001	
BC	411.29	1	411.29	56.04	<0.0001	
A^2	1,078.11	1	1,078.11	146.90	<0.0001	
B^2	183.50	1	183.50	25.00	0.0004	
Residual	80.73	11	7.34			
Lack of Fit	77.68	6	12.95	21.25	0.0021	
Pure Error	3.05	5	0.61			
Cor Total	2,779.84	19	337.39			

*SS: sum of squares; **df: degree of freedom, ***MS: Mean Squares.

were used for experimental investigation. The FSW tools determine the mechanical, weld quality, and micro-structural characteristics of the FSWed joint (Cui, L et al., 2018). FSW tool used for experimentation is AISI H13 tool steel, hardened, and tempered. Because of its high toughness and fatigue resistance, H13 tool steel is perfect for both hot and cold applications. The welding tool for this experiment has been designed and manufactured to have a D/d ratio of 2.5, shoulder diameter of 20 mm, threaded pin diameter of 8 mm with length of 5.8 mm. The reinforcing material used in this investigation is nano alumina (Al_2O_3) with an average particle size of 33 nm and a constant 8% volume fraction. The reinforcement percent of nano alumina has been decided by the number of holes drilled in the FSW plates and volume fraction (Sadeghi, B., et al., 2022). The FSW process is performed in VDF1200 CNC Vertical Milling Center. 20 mm thick mild-steel plates have been in proper dimensional sizes to secure the two dissimilar aluminum plates in the butt position. A backing plate of 20 mm thickness was used underneath the aluminum to protect the milling table from frictional heat and to rigidly support the weld material against the axial force from the welding tool.

2.2 FSW experimental process

Fifteen equally spaced holes of diameter 2 mm and length 4 mm on each edge of both dissimilar plates of aluminum alloys AA 2024-T351 and AA7075-T651 have been drilled and cleaned with acetone to remove the possible grease, dirt, and stains effectively. A volume fraction of 8% Al_2O_3 Nano-powder was mixed with methanol (CH_3OH) of 99% purity, and the resulting thick slurry was charged manually into the 15 drilled lateral holes of both aluminum plates, as shown in Figure 1. The multi-pass FSW was carried out using a VDF- 1200 CNC Vertical Machining Center.

2.3 Experimental design process

Response surface method (RSM) is an effective scientific method for modeling and analyzing problems when many variables influence the response of interest and where the goal is to optimize the parameter (Cui, L et al., 2018). The RSM approach was utilized to assess the relationships between the independent variables and the responses, predict responses, and complete the optimization in the intended range. The statistical model was generated for each response after the FSWed characteristics were measured, and the relationship between the parameters and the FSWed characteristics was assessed. The current study attempted to optimize process parameters by creating a quadratic (2nd order) function to characterize FSW process performance. The equation was then used to establish the process at its optimal setting, which could be achieved through the use of CCD. Furthermore, the CCD proves to be an effective tool for researching the relationships between process factors. The second-order RSM regression model links the process parameters and the responses. The form of the RSM model is shown in Eq. 1 as follows.

$$y = \beta_0 + \sum_{i=1}^{k} \beta_i x_i + \sum_{i=1}^{k} \beta_{ii} x_i^2 + \sum_{i} \sum_{j} \beta_{ij} x_i \quad (1)$$

Where: y is response, β_0 to β_{ij} are coefficients of unknown constant computed from the analysis, x_i are independent variables, k is the quantity of independent variables.

The study employed a Central Composite Design (CCD), the most commonly used and preferred experimental design for RSM (Bhattacharya, S., 2021). A CCD model may have the desired

TABLE 4 ANOVA table for yield strength (MPa).

Source	*SS	**df	***MS	F-value	*p*-value Prob > F	
Model	1788.08	9	198.68	1,242.20	<0.0001	Significant
A-Rotational speed	23.46	1	23.46	146.67	<0.0001	
B-Welding speed	39.80	1	39.80	248.87	<0.0001	
C-Plunge Depth	1.54	1	1.54	9.63	0.0112	
AB	182.54	1	182.54	1,141.33	<0.0001	
AC	109.17	1	109.17	682.56	<0.0001	
BC	151.98	1	151.98	950.25	<0.0001	
A^2	988.34	1	988.34	6,179.53	<0.0001	
B^2	389.41	1	389.41	2,434.80	<0.0001	
C^2	66.12	1	66.12	413.38	<0.0001	
Residual	1.60	10	0.16			
Lack of Fit	0.93	5	0.19	1.37	0.3681	
Pure Error	0.67	5	0.13			
Cor Total	1789.68	19				

TABLE 5 ANOVA table for micro hardness (HRB).

Source	*SS	**df	***MS	F-value	*p*-value Prob > F	
Model	197.88	6	32.98	131.05	<0.0001	Significant
A-Rotational speed	0.72	1	0.72	2.87	0.1138	
B-Welding speed	95.25	1	95.25	378.51	<0.0001	
C-Plunge Depth	6.76	1	6.76	26.88	0.0002	
A^2	20.34	1	20.34	80.83	<0.0001	
B^2	81.96	1	81.96	325.71	<0.0001	
C^2	1.61	1	1.61	6.40	0.0252	
Residual	3.27	13	0.25			
Lack of Fit	2.97	8	0.37	6.22	0.0298	
Pure Error	0.30	5	0.060			
Cor Total	201.15	19				

characteristics of rotatability and orthogonal blocks, depending on the alpha value to reduce the variation in the regression coefficients. The CCD's alpha value (α) is influenced by the total number of experiment trials in the factorial section to preserve rotatability. This study assessed the impact of process variables on the tensile strength (TS), yield strength (YS), and microhardness (MH) of FSWed joints made between dissimilar grades of aluminum alloys, 2024-T351 and 7075-T651. The DoE and analysis of the FSW process are performed with design expert software. Table 1 shows the FSW factors and levels. The FSW parameter ranges were considered for current studies based on CNC machine centers with operating ranges and a comprehensive literature survey (Teja and Srinivasan, 2024). Twenty experimental factors and levels were used, and the experimental results of FSW of dissimilar aluminum alloys are shown in Table 2.

2.4 Testing and characterization

Material testing and characterization are crucial in evaluating the FSWed joints' quality attributes. The study employed the Tensile Strength (MPa), Yield Strength (MPa), and Micro-hardness (HRB) tests for mechanical properties analysis. The Scanning Electron Microscope (SEM) and optical microscope were used to investigate the microstructure and topographical analysis.

2.4.1 Tensile testing

The ASTM E8/E8M sub-size standard was used for tensile test specimens by wire electro-discharging machining (WEDM) technique. The tensile tests are performed in UTM machine.

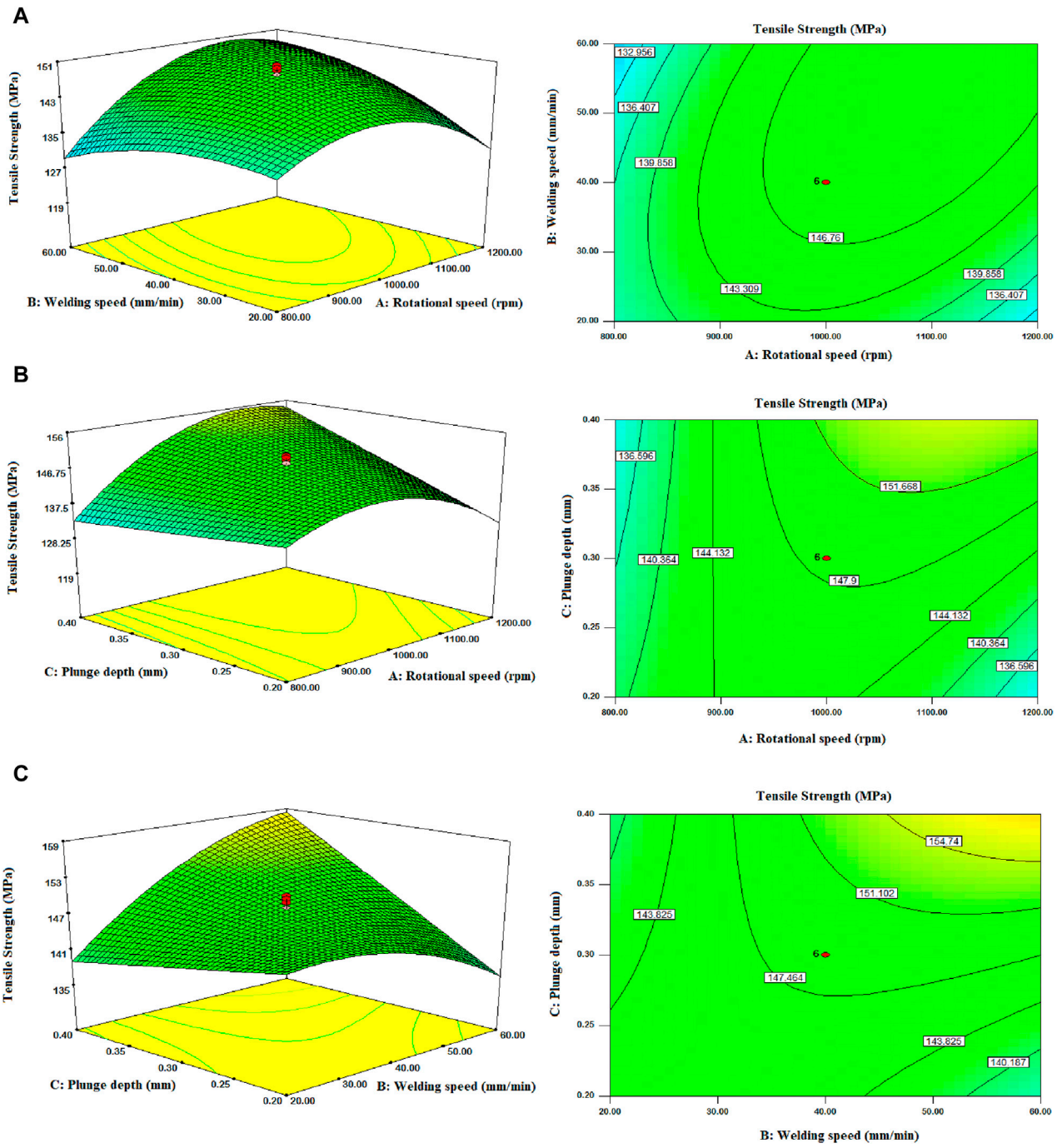

FIGURE 2
(A–C) 3D graphs 2D contour plots showing interaction effect of three factors rotational speed, welding speed and plunge depth on Tensile strength (MPa).

2.4.2 FSWed joint -hardness test

The Rockwell hardness tester (HRB scale) is used with a 1/16" (1.5875 mm) diameter ball indenter. The hardness test was CONDUCTED on the benchtop digital superficial Rockwell hardness tester of model HRMS-45 with ASTM E18 standards of preliminary test force 98 N and 981 N of total test force. The average values of the micro-hardness result in the HRB scale are shown in Table 2.

2.4.3 Microscopic samples preparation

The microscopic samples prepared were polished with the help of 320, 400, 600, 800, 1,200, and 2000 grit-sized silicon carbide (SiC) abrasive papers, followed by a polishing machine. Next, the samples from the welded joint were cleaned with Keller's etching chemicals as per ASTM standard E407.

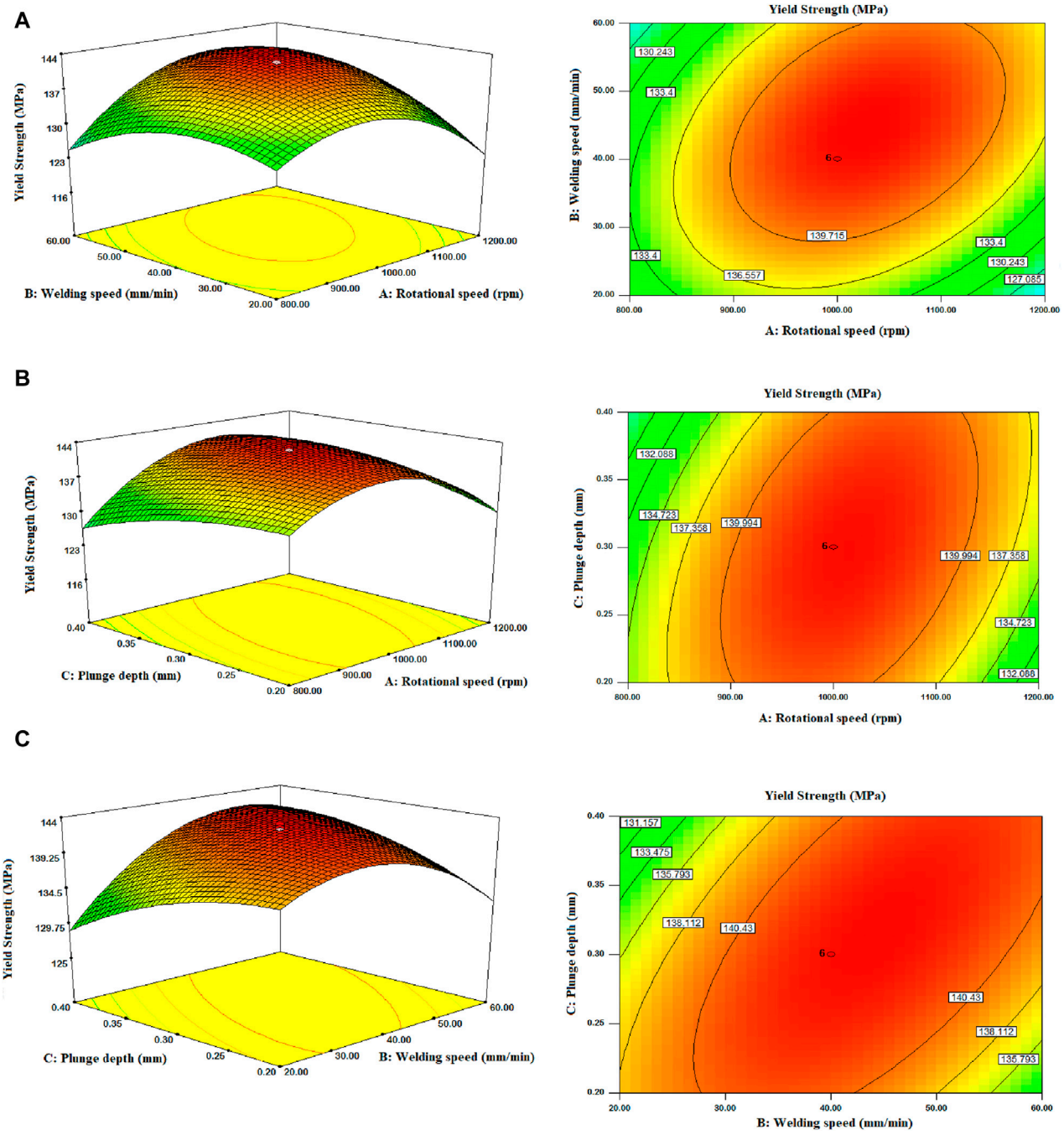

FIGURE 3
(A–C) 3D graphs 2D contour plots showing interaction effect of three factors rotational speed, welding speed and plunge depth on Yield Strength (MPa).

3 Results and discussion

3.1 Model equations for FSW

A regression model describes the interaction among several independent factors and a dependent variable. Hence, the model formulates the equations to predict responses. The final model equations (Eqs 2–4) created predicts the UTS, YS, and Microhardness of the AA 2024-T351 and AA 7075-T651 DFSW joints. The statistical significance of any differences between the means of multiple groups is ascertained by applying Analysis of Variance (ANOVA).

Tensile strength, yield strength, and microhardness are three responses that are significantly affected by the interaction of process parameters. As a result, the CCD approach was chosen for process parameter optimization. CCD provides the mathematical model used for predicting the weld's tensile strength, yield strength, and microhardness, shown in Eqs 2–4. In order to determine the significant factor, the ANOVA approach investigated the parametric effect. It establishes that

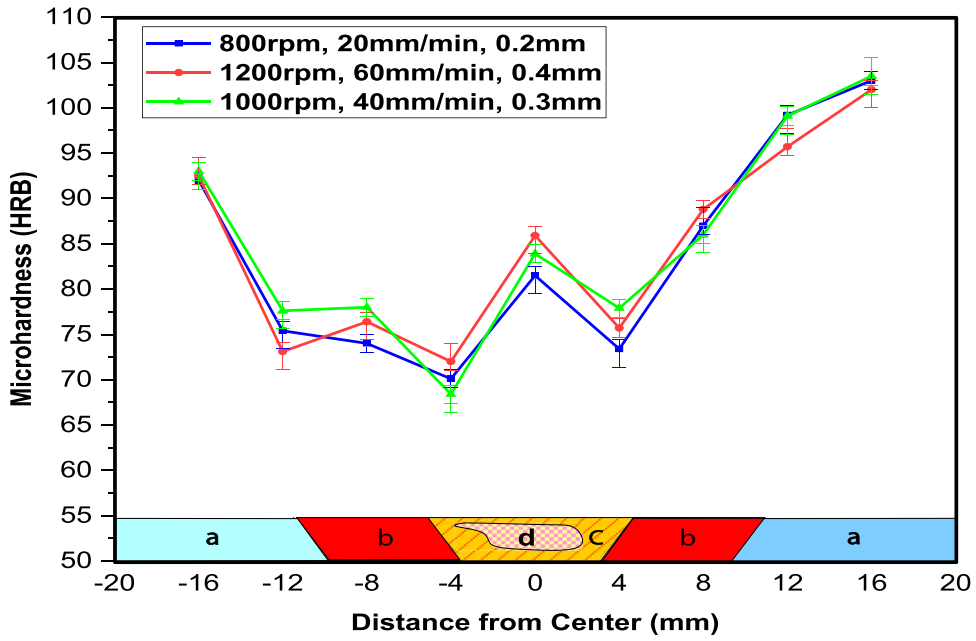

FIGURE 4
The hardness profiles of the FSWed joint.

responses are dependent on the parameters. Comparing the mean square against all experimental data, which yields the ANOVA test, resulted in Tables 3–5, examining each significant component's importance and interaction. Insignificant factors are removed from ANOVA by a backward elimination process. The accuracy of the models created based on the data was assessed using an F-test of ANOVA, and the results are shown in Tables 3–5. According to the assessments, these values represented the regression model's best fit at a 95% confidence level, suggesting that the statistical models used were accurate.

$$Y_{TS} = 148.53 + 3.54A + 2.48B + 3.75C + 5.82\,AB + 6.89AC + 7.17BC - 8.61A^2 - 3.55\,B^2 \quad (2)$$

$$Y_{YS} = 142.58 + 1.31A + 1.71B - 0.34C + 4.78\,AB + 3.69AC + 4.36BC - 8.28A^2 - 5.20\,B^2 - 2.14C^2 \quad (3)$$

$$Y_{MH} = 88.36 + 023A + 2.64B + 0.70C - 1.19A^2 - 2.38\,B^2 - 0.33C^2 \quad (4)$$

Interaction between these three factors significantly affects tensile stress. Additionally, the tool rotational and welding speeds have quadratic effects corresponding to their significance. The yield strength is directly impacted by all three input factors, in order of significance, as shown by Eq. 3, additionally, interaction and quadratic effects are based on their relative relevance. As shown in Eq. 4, the linear effects of the following input variables and quadratic effects of all three factors significantly affect microhardness.

3.2 FSW parameters effect on tensile strength (TS)

ANOVA determines whether the various factors significantly affect the response variables. According to the ANOVA Table 3, the main interaction and high-ordered model terms A^2 and B^2 significantly influence the tensile strength. The *p*-value from the ANOVA Table 3 is ≤ 0.05, showing a statistically significant model. Hence, this smaller *p*-value indicates a significant difference among the response variable levels. The second-order response surfaces are fitted accurately by the experimental values.

The tensile values increase while the tool rotation increases; the highest tensile value is 170 MPa, obtained at high levels of FSW conditions such as 1,200 rpm, 60 mm/min, and 0.4 mm. It is because of the significant grain refinement brought on by the FSW process's sustained dynamic recrystallization and extreme plastic deformation. The lowest tensile value of 119.2 MPa was found at 663 rpm. The tool rotation controls the level of heat developed during the FSW process (Zhang Z. et al., 2014; Dawood et al., 2015). The heat developed in FSW influences the material mixture and deformation due to plasticity (Kisuka F. et al., 2024; Salih et al., 2023). Due to inadequate material mixing, Al_2O_3 clustered, and the link between Al_2O_3 and the matrix material was weak in the FSWed joints manufactured at tool rotation 700 rpm (Chen X G et al., 2009).

At medium-level welding conditions, the tensile value is 150 MPa. The 3D surface and contour plot graphs in Figures 2A–C illustrate the relationship between rotational speed-welding speed and plunge depth on the tensile strength. The 3D and contour plot (Figures 2A, B) shows that the tensile strength increases while increasing the rotational speed, and similarly, the welding speed and plunge depth increase the tensile strength, as shown in Figure 2C. The changes in tool penetration depth, welding speed, and tool rotating speed can also alter the frictional and stirring conditions, impacting the joint's tensile strength (Vahdati M. et al., 2020). Additionally, the

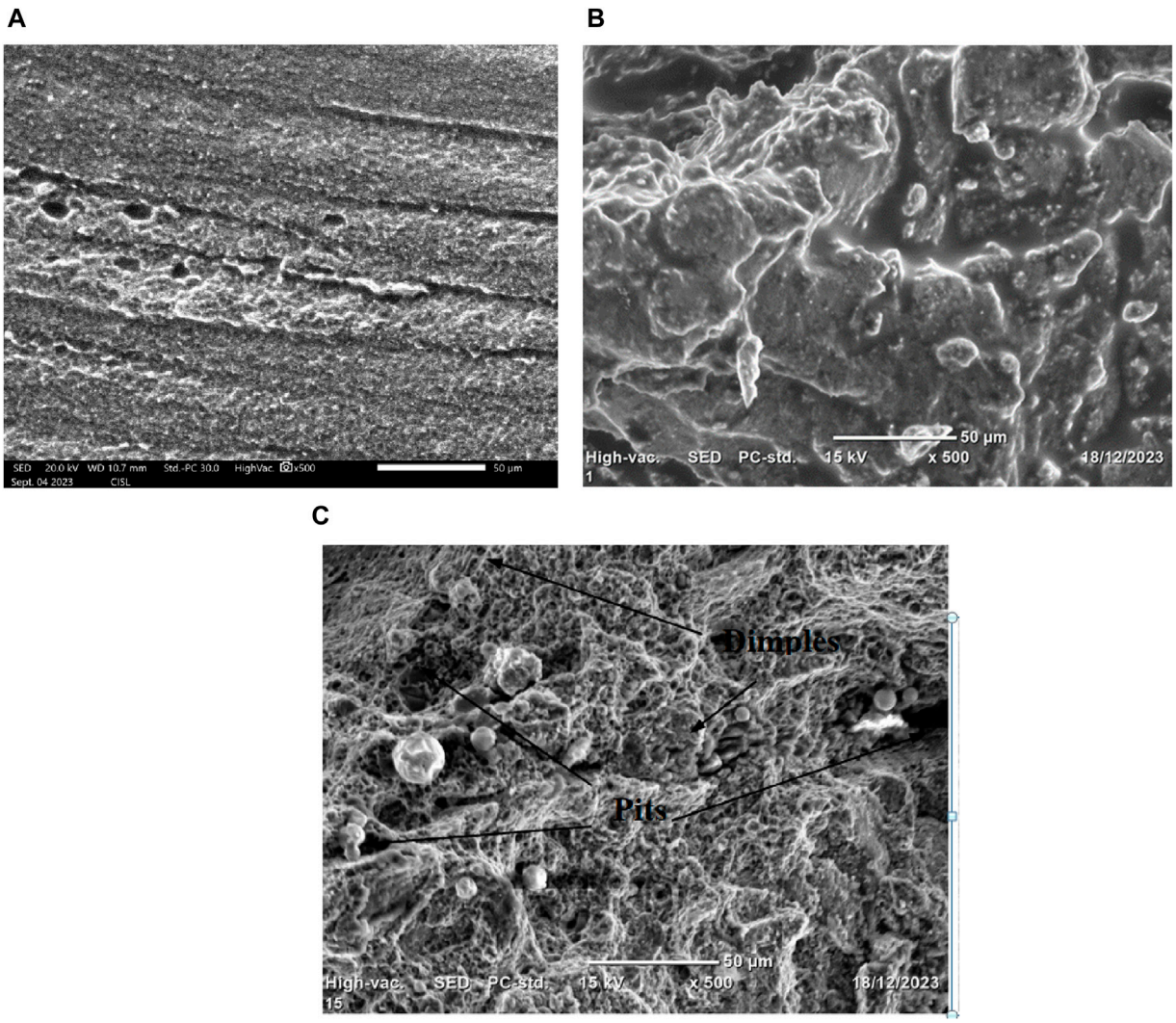

FIGURE 5
(A–C) SEM images of fractured surface at low (800 rpm, 20 mm/min and 0.2 mm), middle (1,000 rpm, 40 mm/min and 0.3 mm) and high (1,200 rpm, 60 mm/min and 0.4 mm) FSW conditions.

tensile strength improves as the welding speed increases because of adequate heating and material agitation (Sabari S. et al., 2016).

The FSWed joint formed at 1,100 rpm tool rotation, 40 mm/min traversal speed with 10% Al_2O_3 nanoparticles demonstrated the enhancement of mechanical performance resulting from microstructure refinement and production of strain-free refined grains during the DRX mechanism (Jain and Mishra, 2022b). Significant strain evolved at an improved RS of 1,100 rpm, which led to the observation of homogeneously dispersed Al_2O_3 and appropriate material mixing. The absence of Al_2O_3 clustering indicates excellent bonding between the matrix and Al_2O_3. Higher RS values improved particle mobility (Palanivel R et al., 2016). The pinning action of the Al_2O_3 particles enhances the nucleation sites and prevents grain formation (Srivastava M et al., 2019). The greater pinning action with a higher percentage of more evenly dispersed Al_2O_3 boosted grain refinement (Azizieh M et al., 2011).

3.3 FSW parameters effect on yield strength

The yield strength of the Al_2O_3 nanoparticle-reinforced dissimilar aluminum alloy FSWed joints was investigated. The main interaction term and high-ordered model terms A^2, B^2, and C^2 significantly influence the yield strength given in Table 4. The relationship between factors on yield strength is shown by the 3D surface and contour graphs in Figures 3A–C. The highest yield strength is obtained by modifying the values of the tool rotating speed and welding speed in the range of maximum level, as shown in Figure 3A. Figure 3A illustrates how to achieve the optimum yield strength by varying the tool rotating speed and welding speed within the maximum level range. Accordingly, the yield strength increases while the rotating speed increases from 800 to 1,200 rpm. Here, frictional heat is increased by increasing the tool's spinning speed. Alternatively, the yield strength increases as a result of more effective material mixing in the joint seam due to the frictional heat produced

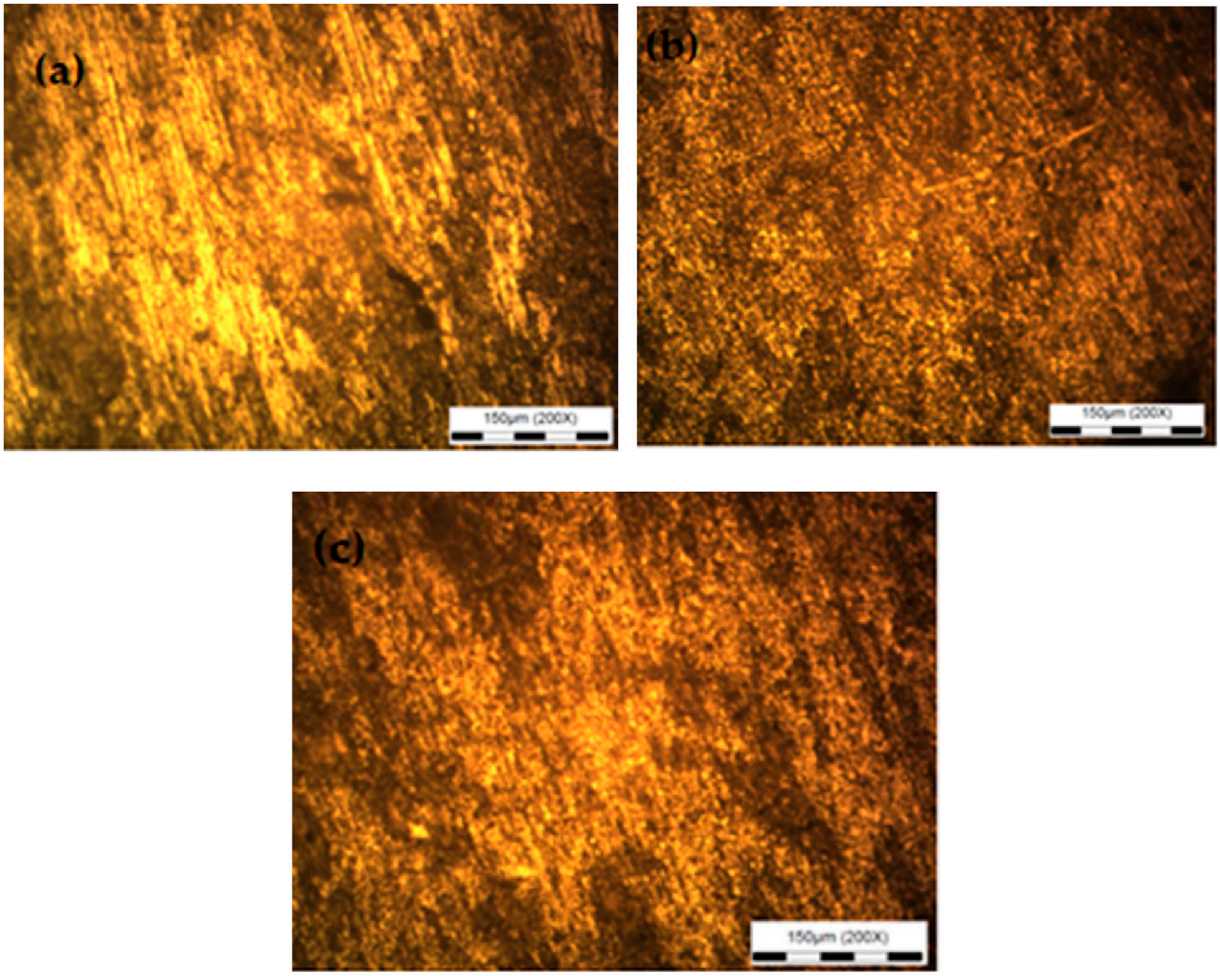

FIGURE 6
(A–C) Optical Microscopic images [WNZ] at low (800 rpm, 20 mm/min and 0.2 mm), middle (1,000 rpm, 40 mm/min and 0.3 mm) and high (1,200 rpm, 60 mm/min and 0.4 mm) FSW conditions.

by expanding the tool's shoulder diameter and the workpiece's contact surface. Both the combined effect of welding speed and tool plunge depth show a similar tendency, as shown in Figures 3B, C. The yield strength is more affected by the combined influence of traverse speed and tool speed (Bhojan et al., 2016). Thus, the yield strength will increase if the welding and rotating speed increase. In this case, frictional heat increases as the tool's rotating speed increases (Vahdati, M., et al., 2020). In contrast, higher yield strength is produced because of the more compelling material mixing in the joint seam caused by the frictional heat generated by a higher plunge depth. The highest yield strength is obtained at high levels of FSW conditions such as 1,200 rpm, 60 mm/min, and 0.4 mm. The lowest yield strength, 117 MPa, was found at 663 rpm, 40 mm/min, and 0.3 mm, respectively.

3.4 The FSW parameters effect on micro-hardness

The ANOVA table of hardness is shown in Table 5. The weld nugget zone's hardness could potentially have been claimed to be caused by the dispersion and grain refinement of Al_2O_3 particles within the WNZ. The heat input during FSW was found to be associated with the refined grain size in the WNZ. The hardness values vary from 77.1 HRB to 89 HRB of the dissimilar aluminum alloys AA 2024-T351 and AA 7075-T651. Table 2 displays the mean micro-hardness value at the midpoint of the weld zone for different reinforced joints. The maximum hardness of 89 HRB was found at high levels of FSW conditions such as 1,200 rpm, 60 mm/min, and 0.4 mm. The lowest micro-hardness values, 77.1 HRB, were 1,000 rpm, 6.36 mm/min, and 0.3 mm. Figure 4 shows the variation of the resulting micro-hardness values Al_2O_3 Nanoparticle reinforced FSWed joints.

The welded joint's microhardness is typically predicted to be higher than the base materials. Microhardness increases during the FSW process due to intense plastic deformation and grain refining. Research findings indicate that the microhardness values of FSWed joints of AA2024 and AA7075 may vary between 77 and 89 HRB, contingent upon the particular FSW parameters utilized. The microhardness values typically result from tool rotation and traverse speed. The FSW process's increased plastic deformation and grain refining are the main causes. These parameters influence

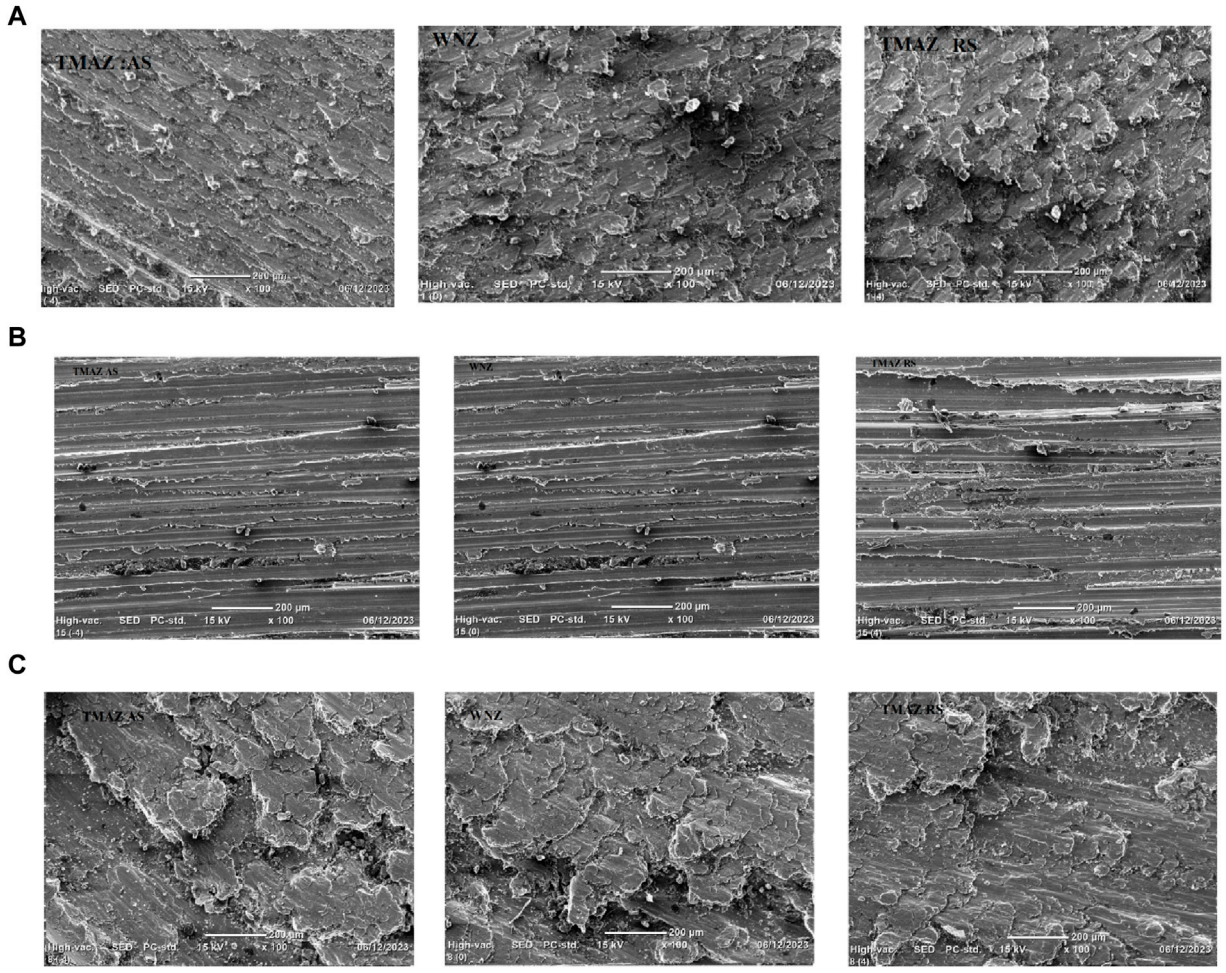

FIGURE 7
(A–C) SEM images at surface of weld area at low (800 rpm, 20 mm/min and 0.2 mm), middle (1,000 rpm, 40 mm/min and 0.3 mm) and high (1,200 rpm, 60 mm/min and 0.4 mm) FSW conditions [TMAZ (AS); WNZ; TMAZ (RS)].

the degree of heat input, the subsequent microstructural alterations, and ultimately, the hardness of the joint is affected. The hardness enhancement due to nano Al_2O_3 has a high joint density and exhibited a greater tensile strength than the joint made with TiO_2 nanoparticles (Singh et al., 2020). Since nano-sized particles were embedded in the WNZ, there was a more noticeable increase in microhardness and wear characteristics compared to joints without reinforcement under the same processing conditions (Singh et al., 2020). Increased grain refinements by nano Al_2O_3 were responsible for improved mechanical properties (Rani et al., 2022).

3.5 Microstructural investigations

Scanning Electron Microscope (SEM) photographs of the Al_2O_3 nanoparticle-reinforced FSWed joint's fractured surface morphology are displayed in Figure 5. SEM is an imaging technique that images a material's surface using an electron beam. SEM images reveal that the specimens' fracture surfaces include a variety of characteristics, such as shear lips, pits, and cracks. More microvoids were observed in low-level FSW conditions, as shown in Figure 5A. Little cracks discovered in images are displayed in Figure 5B. FSWed joints created at the rotational speed of 1,200 rpm and welding speed of 60 mm/min, 0.4 mm plunge depth produce consistent dispersion with substantial fragmentation of particles obtained and also particles agglomeration to be absent. The closer combination of such input parameters also enhances the mechanical parameters like tensile strength, % elongation, and micro-hardness (Jain and Mishra, 2022b). A significant volume fraction of different intermetallic particles can be found in al-alloy. Al_2O_3-based intermetallics are inclusions and particles in brittle phases distributed throughout the Al-matrix. Once plastic deformation occurs, the voids are initiated or nucleated mainly at the grain boundaries due to the incompatibility of the Al-matrix and intermetallic particles with differing characteristics. These features make it easy to investigate the mechanisms underlying ductile fracture and damage evolution. The Al-alloy's *in situ* tensile experiments demonstrate that, for ductile materials, dimple-dominant fracture typically happens as depicted in Figure 5C (Li and Fu (2019). The specimens were fractured ductile, as indicated by the dimples that predominated on the fracture surfaces (Figure 5C).

TABLE 6 Optimal FSW conditions by RSM.

Optimum combination input parameters		Responses	Predicted values		Experimental values
			Desirability approach	ANN	
Rotational speed	1,146 rpm	Tensile strength (MPa)	165.65	171.71	169
Welding speed	60 mm/min	Yield strength (MPa)	143.69	141.92	145
Plunge depth	0.4 mm	Microhardness (HRB)	88.5	86.03	89

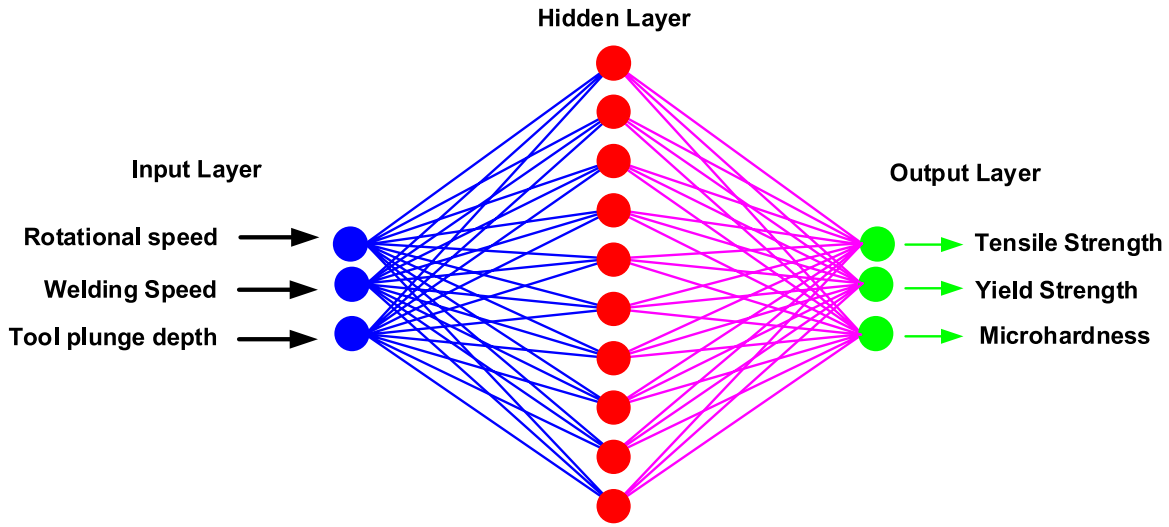

FIGURE 8
Architecture of ANN.

Figure 6 shows the optical microscope image of WNZ (a) lower input parameters, (b) medium input parameters, and (c) higher input parameters. According to the microscopic images, the size of the grain particles is fine at medium and higher levels. The homogenous distribution of the Al_2O_3 nanoparticle is better when compared with low-level conditions. Adding nanoparticles to aluminum alloys AA2024 and AA7075 during FSW can refine grain, enhancing the joint's strength and ductility. Similar results showed that the scattered SiC particles in the WNZ had a zener pinning effect and dynamic recrystallization, which refined the grains (Moustafa E B. et al., 2023). Results showed a pinning effect of scattered SiC particles in the WNZ and DRX, which led to grain refinement, causing an impact on the micro-hardness and tensile strength. Accordingly, higher ultimate tensile strength and maximum microhardness were recorded using 1,100 rpm tool rotation; 40 mm/min weld speed, and a SiC particle of 10% (Jain and Mishra, 2022b). Potential factors contributing to these changes include grain modification, ceramic particles in the interfaces, high applied strain that modifies the atomic network parameters very little, and the lamellar structure of the treated Al 1,050 in higher passes (Tayyebi et al., 2019). The primary distinction between raw material and processed Al layers is that dimples with the ARB process are smaller and shallower. This pattern has also been observed in prior comparable studies, which have found that using ARB techniques does not modify the failure mechanism for different Al alloys but rather affects the shape, quantity, and size of dimples (Rahmatabadi, D et al., 2019).

Figures 7A–C show the SEM images of surface topography at different FSW conditions with WNZ and TMAZ of the advancing and retracting sides of the weld joint. The welded zone displays the vortex flow pattern, and the mixed flow region consists of the AA2024 and AA7075 lamellae structures. The two alloys mix and penetrate deeply in this area, causing the plasticized material to experience extreme superplastic flow and turbulent intercalation patterns. Both alloys experience intense plastic deformation and *in-situ* extrusion due to the stirring tool action. The plasticized material is transferred layer by layer to form a lamellae structure. Especially at higher WS, the mixing is much more successful when the AA2024 is positioned on the AS, as shown in Figure 7C.

3.6 Desirability approach for optimization

According to Myers et al. (2016), the desirability function approach is famous for multiple response optimization processes. This procedure finds the highest suitable response values under operating conditions x. This method transforms all the responses into distinct DFs (di) with a scale factor ranging from 0 to 1. If the

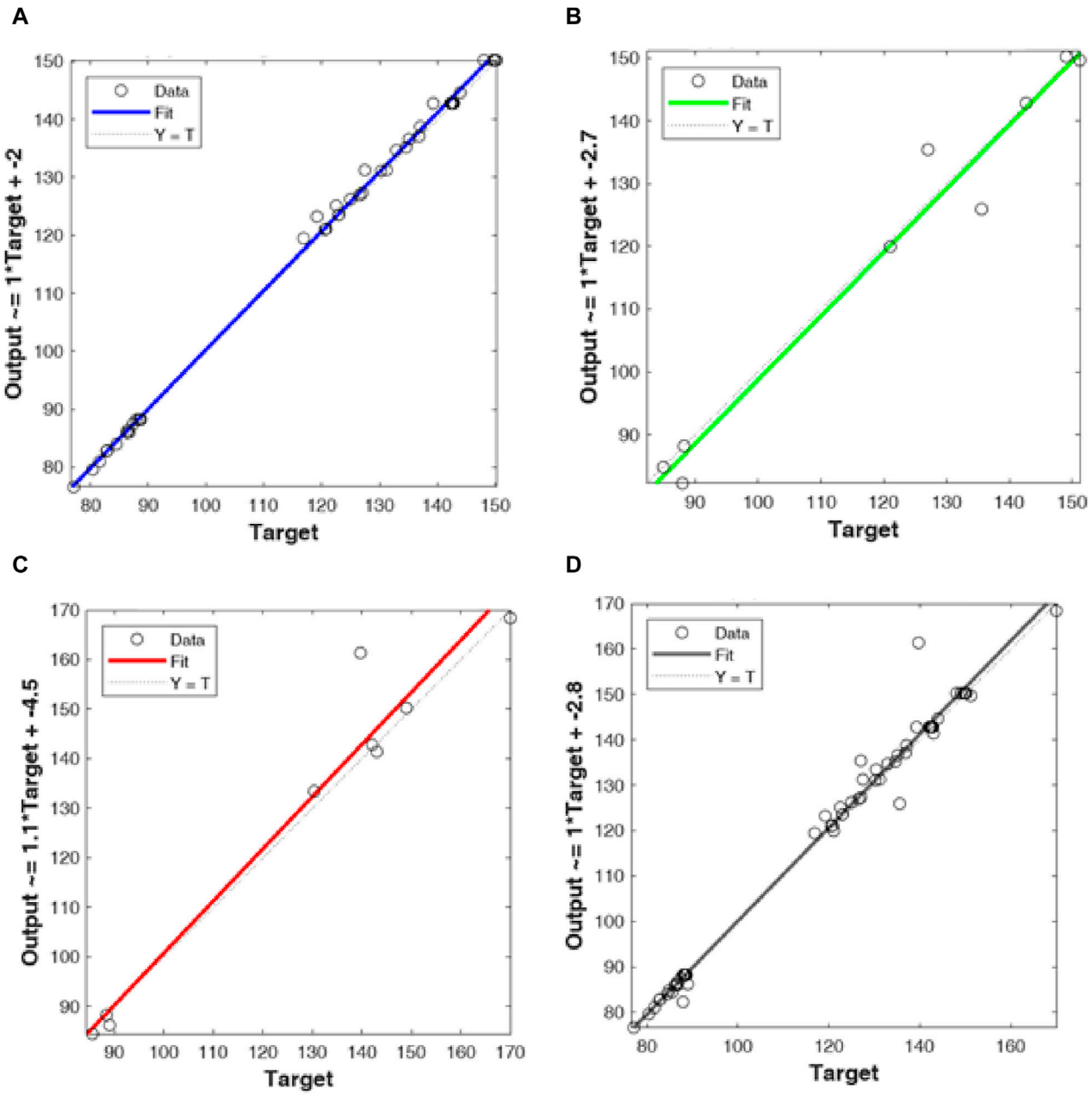

FIGURE 9
(A–D) Comparison of measured and predicted data for **(A)** training data, **(B)** validation **(C)** test data, **(D)** overall data.

desirability value is zero, the predicted value is deemed entirely undesirable, and the value is one denoted by a more desirable. These functions are organized by defining the values from the experiments as the desired outcome based on objective function minimization or maximization of response (y_i) (Derringer and Suich, 1980). Equation 5 determines each variable's composite desirability (D) after the individual desirability has been determined. The predicted responses are weighted as one response considered maximizing. Individual desirability (di) is then determined using Eq. 6.

$$D = (d_1, d_2, d_3 \ldots\ldots\ldots\ldots\ldots d_n)^{\frac{1}{n}} \tag{5}$$

Individual desirability for maximization as:

$$d_i = \begin{cases} 0 & y_i < L \\ \left(\dfrac{y_i - L}{T - L}\right)^r & L \le y_i \le T \\ 1 & y_i > T \end{cases} \tag{6}$$

The optimum parameters for the proposed desirability function are a tool rotation at 1,146 rpm, a transverse speed at 60 mm/min, and a plunge at 0.4 mm given in Table 6. These combinations produced a maximum performance in yield strength of 143.69 MPa, tensile strength of 165.65 MPa, and a hardness value of 88.5 HRB. The confirmation experiments are conducted for the predicted parameter values. The predicted optimal parameters produced joints gave tensile strength of 169 MPa, yield strength of

145 MPa, hardness of 89 HRB, and error values of less than 5% at a confidence level of 95%.

3.7 ANN model for FSW process

ANN models have been widely used as predictive strategies because of their affordability, relative ease of understanding, and capacity to be trained utilizing data gathered from these intricate manufacturing processes (Essa, A. R et al., 2023; Pany et al., 2001). An ANN is made up of three layers: the input layer, the hidden layer, and the output layer, as shown in Figure 8. The input layer contains all of the input parameters. The input layer's data is processed by the hidden layer, and the subsequent output layer computes the subsequent output vector. The basic sequential computation elements of an ANN are modeled from the biological nervous system. An ANN's neuron is its fundamental building block. Synapses, which connect neurons, are linked by a weight factor that is tied to each synapse. Using a single hidden layer, the Levenberg-Marquardt algorithm was applied in this study. Therefore, the network topology was composed of three neuronal outputs with a linear activation function, a logistic sigmoid, ten hidden neurons with a nonlinear activation function, and three input neurons. The 14 sets of data were used for training, and each three sets of data were used for the testing and validation process. Figures 9A–D illustrates predicted values are well agree with the measured data. Based on R-values 0.9991, 0.9754, 0.9846 for training, testing and validation respectively, the results demonstrate a high degree of similarity between the measured and predicted data sets. The ANN predicted, and experimental values are given in Table 6.

4 Conclusion

This study examined the reinforcing Al_2O_3 Nano particle affects the mechanical and micro-structural properties of FSWed joints of dissimilar Al alloy AA2024-T351 and AA7075-T651. The following important findings were drawn from the investigations.

- The resulting welded joint with higher mechanical properties was due to the microstructure refinement via the zener pinning effect.
- Process factors can favorably influence the weld's tensile properties. More heat is produced when the tool's rotation, welding speed and plunge depth are increased, which significantly impacts the weld joint's mechanical characteristics.
- ANOVA shows that FSW factors are statistically significant and affect the response of FSW. The desirability function was used to predict optimal FSW process conditions; the predicted conditions were a tool rotation of 1,146 rpm, 60 mm/min of weld speed, and a plunge depth of 0.4 mm.
- Considering the optimal conditions and carefully analyzing FSWed joints produced with higher tensile properties yield strength of 145 MPa, tensile strength of 169 MPa, and a microhardness of 89 HRB with a tool rotation at1146 rpm, and a weld speed at 60 mm/min and plunge depth at 0.4 mm.
- ANN and desirability approach employed for prediction of FSW of Al alloy, both model has a good fit with experimental values and error values has less than five percentages.
- To further extend its excellence in using high-temperature materials, composites, and polymers, the research community must put much effort into developing the technology to overcome various obstacles. Addition of various nanoparticles such as boron carbide, silicon carbide, CNT, and AL_2O_3 at different volume percentages in FSW using a variety of Al alloys.
- One of the main obstacles preventing the FSW process from being used on high-softening-temperature materials is the necessity for tool materials. Tool profiles and dimensions of additive mixed FSW also need to be explored. The authors prompt further studies in more affordable tool materials and the adoption of current CNC machines to exploit the immense potential of the FSW process.

Data availability statement

The original contributions presented in the study are included in the article/Supplementary Material, further inquiries can be directed to the corresponding author.

Author contributions

GG: Conceptualization, Data curation, Investigation, Methodology, Validation, Writing–original draft. SP: Conceptualization, Data curation, Formal Analysis, Investigation, Methodology, Supervision, Validation, Visualization, Writing–review and editing. BS: Supervision, Visualization, Writing–review and editing. RČ: Methodology, Resources, Visualization, Writing–review and editing.

Funding

The author(s) declare that no financial support was received for the research, authorship, and/or publication of this article.

Acknowledgments

Authors are sincerely thankful to Addis Ababa Science and Technology University (AASTU) for laboratory and technical support.

Conflict of interest

The authors declare that the research was conducted in the absence of any commercial or financial relationships that could be construed as a potential conflict of interest.

Publisher's note

All claims expressed in this article are solely those of the authors and do not necessarily represent those of their affiliated

organizations, or those of the publisher, the editors and the reviewers. Any product that may be evaluated in this article, or claim that may be made by its manufacturer, is not guaranteed or endorsed by the publisher.

References

Abnar, B., Gashtiazar, S., and Javidani, M. (2023). Friction stir welding of non-heat treatable Al alloys: challenges and improvements opportunities. *Crystals* 13 (4), 576. doi:10.3390/cryst13040576

Ahmadi, M., Pahlavani, M., Rahmatabadi, D., Marzbanrad, J., Hashemi, R., and Afkar, A. (2022). An exhaustive evaluation of fracture toughness, microstructure, and mechanical characteristics of friction stir welded Al6061 alloy and parameter model fitting using response surface methodology. *J. Mater. Eng. Perform.* 31, 3418–3436. doi:10.1007/s11665-021-06461-1

Aminzadeh, A., Parvizi, A., Safdarian, R., and Rahmatabadi, D. (2021). Comparison between laser beam and gas tungsten arc tailored welded blanks via deep drawing. *Proc. Institution Mech. Eng. Part B J. Eng. Manuf.* 235 (4), 673–688. doi:10.1177/0954405420962391

Azizieh, M., Kokabi, A. H., and Abachi, P. (2011). Effect of rotational speed and probe profile on microstructure and hardness of AZ31/Al2O3 nanocomposites fabricated by friction stir processing. *Mater. Des.* 32 (4), 2034–2041. doi:10.1016/j.matdes.2010.11.055

Bhattacharya, S. (2021). "Central composite design for response surface methodology and its application in pharmacy," in *Response surface methodology in engineering science*. IntechOpen. doi:10.5772/intechopen.95835

Bhojan, A., Senthilkumar, N., and Deepanraj, B. (2016). Parametric influence of friction stir welding on cast Al6061/20% SiC/2% MoS2 MMC mechanical properties. *Appl. Mech. Mater.* 852, 297–303. doi:10.4028/www.scientific.net/amm.852.297

Boopathi, M. M., Arulshri, K. P., and Iyandurai, N. (2013). Evaluation of mechanical properties of aluminium alloy 2024 reinforced with silicon carbide and fly ash hybrid metal matrix composites. *Am. J. Appl. Sci.* 10 (3), 219–229. doi:10.3844/ajassp.2013.219.229

Ceschini, L., Minak, G., and Morri, A. (2006). Tensile and fatigue properties of the AA6061/20 vol% Al2O3p and AA7005/10 vol% Al2O3p composites. *Compos. Sci. Technol.* 66 (2), 333–342. doi:10.1016/j.compscitech.2005.04.044

Chen, X. G., Da Silva, M., Gougeon, P., and St-Georges, L. (2009). Microstructure and mechanical properties of friction stir welded AA6063–B4C metal matrix composites. *Mater. Sci. Eng. A* 518 (1-2), 174–184. doi:10.1016/j.msea.2009.04.052

Cui, L., Zhang, C., Liu, Y. C., Liu, X. G., Wang, D. P., and Li, H. J. (2018). Recent progress in friction stir welding tools used for steels. *J. Iron Steel Res. Int.* 25, 477–486. doi:10.1007/s42243-018-0066-7

Dawood, H. I., Mohammed, K. S., Rahmat, A., and Uday, M. B. (2015). Microstructural characterizations and mechanical properties in friction stir welding technique of dissimilar (Al-Cu) sheets. *J. Appl. Sci. Agric.* 10 (5), 149–158.

Derringer, G., and Suich, R. (1980). Simultaneous optimization of several response variables. *J. Qual. Technol.* 12 (4), 214–219. doi:10.1080/00224065.1980.11980968

Essa, A. R., Ahmed, M. M., Aboud, A. R., Alyamani, R., and Sebaey, T. A. (2023). Prediction of tool eccentricity effects on the mechanical properties of friction stir welded AA5754-H24 aluminum alloy using ANN model. *Materials* 16 (10), 3777. doi:10.3390/ma16103777

Fang, Y., Jiang, X., Mo, D., Zhu, D., and Luo, Z. (2019). A review on dissimilar metals' welding methods and mechanisms with interlayer. *Int. J. Adv. Manuf. Technol.* 102, 2845–2863. doi:10.1007/s00170-019-03353-6

Gebreamlak, G., Palani, S., Sirhabizu, B., Atnaw, S. M., and Gebremichael, E. (2022). Dissimilar friction stir welding process-a review. *Adv. Mater. Process. Technol.* 8 (4), 3900–3922. doi:10.1080/2374068X.2022.2036446

Hassan, A. S., Moustafa, E. B., and Mohamed, S. S. (2023). Impact of welding processing parameters on the microstructure grain refinement and hardness behavior of the aluminum AA1050. *Egypt. J. Chem.* 66 (12), 291–302. doi:10.21608/EJCHEM.2023.187195.7448

He, T., Ertuğrul, O., Ciftci, N., Uhlenwinkel, V., Nielsch, K., and Scudino, S. (2019). Effect of particle size ratio on microstructure and mechanical properties of aluminum matrix composites reinforced with Zr48Cu36Ag8Al8 metallic glass particles. *Mater. Sci. Eng. A* 742, 517–525. doi:10.1016/j.msea.2018.11.007

Jain, S., and Mishra, R. S. (2022a). Effect of Al2O3 nanoparticles on microstructure and mechanical properties of friction stir-welded dissimilar aluminum alloys AA7075-T6 and AA6061-T6. *Proc. Institution Mech. Eng. Part E J. Process Mech. Eng.* 236 (4), 1511–1521. doi:10.1177/09544089211065534

Jain, S., and Mishra, R. S. (2022b). Microstructural and mechanical behavior of micro-sized SiC particles reinforced friction stir processed/welded AA7075 and AA6061. *Silicon* 14 (16), 10741–10753. doi:10.1007/s12633-022-01716-5

Kisuka, F., Hare, C., and Wu, C. Y. (2024). Heat generation induced by plastic deformation during particle normal impact. *Int. J. Impact Eng.* 184, 104831. doi:10.1016/j.ijimpeng.2023.104831

Kumar, K. S. A., Murigendrappa, S. M., and Kumar, H. (2019). Experimental investigation on effects of varying volume fractions of SiC nanoparticle reinforcement on microstructure and mechanical properties in friction-stir-welded dissimilar joints of AA2024-T351 and AA7075-T651. *J. Mater. Res.* 34 (7), 1229–1247. doi:10.1557/jmr.2018.445

Kundu, A. K., Gupta, M. K., Rajput, N. S., and Rathore, R. (2022). Adhesive assisted TiB2 coating effects on friction stir welded joints. *Sci. Rep.* 12 (1), 17894. doi:10.1038/s41598-022-21281-6

Li, H., and Fu, M. (2019). *Deformation-based processing of materials: behavior, performance, modeling, and control*. Elsevier.

Mirjavadi, S. S., Alipour, M., Emamian, S., Kord, S., Hamouda, A. M. S., Koppad, P. G., et al. (2017). Influence of TiO2 nanoparticles incorporation to friction stir welded 5083 aluminum alloy on the microstructure, mechanical properties and wear resistance. *J. Alloys Compd.* 712, 795–803. doi:10.1016/j.jallcom.2017.04.114

Morales, C., Merlin, M., Fortini, A., Garagnani, G. L., and Miranda, A. (2022). Impact behaviour of dissimilar AA2024-T351/7075-T651 FSWed butt-joints: effects of Al2O3-SiC particles addition. *Frat. Ed. Integrità Strutt.* 16 (60), 504–515. doi:10.3221/IGF-ESIS.60.34

Moustafa, E. (2017). Effect of multi-pass friction stir processing on mechanical properties for AA2024/Al2O3 nanocomposites. *Materials* 10 (9), 1053. doi:10.3390/ma10091053

Moustafa, E. B., Sharaf, M., Alsoruji, G., Mosleh, A. O., Mohamed, S. S., and Hussein, H. (2023). Microstructural and mechanical characterization of the dissimilar AA7075 and AA2024 aluminum alloys reinforced with different carbide particles welded by friction stir welding. *J. Compos. Sci.* 7 (11), 448. doi:10.3390/jcs7110448

Myers, R. H., Montgomery, D. C., and Anderson-Cook, C. M. (2016). *Response surface methodology: process and product optimization using designed experiments*. John Wiley & Sons.

Palanivel, R., Dinaharan, I., Laubscher, R. F., and Davim, J. P. (2016). Influence of boron nitride nanoparticles on microstructure and wear behavior of AA6082/TiB2 hybrid aluminum composites synthesized by friction stir processing. *Mater. Des.* 106, 195–204. doi:10.1016/j.matdes.2016.05.127

Pany, C. (2021a). Cylindrical shell pressure vessel profile variation footprint in strain comparison of test data with numerical analysis. *Liq. Gaseous Energy Resour.* 1 (2), 91–101. doi:10.21595/lger.2021.22163

Pany, C. (2021b). Estimation of correct long-seam mismatch using fea to compare the measured strain in a non-destructive testing of a pressurant tank: a reverse problem. *Int. J. Smart Veh. Smart Transp. (IJSVST)* 4 (1), 16–28. doi:10.4018/ijsvst.2021010102

Pany, C., Sundaresan, M. K., Rao, B. N., Sivasubramonian, B., and Nair, N. J. (2012). On the bursting of an HSLA steel rocket motor case during proof pressure testing. *Steel Grips J. Steel Relat. Mater. Appl.* 10, 434–438.

Pany, C., Tripathy, U. K., and Misra, L. (2001). Application of artificial neural network and autoregressive model in stream flow forecasting. *JOURNAL-INDIAN WATERWORKS Assoc.* 33 (1), 61–68.

Rahmatabadi, D., Shahmirzaloo, A., Hashemi, R., and Farahani, M. (2019). Using digital image correlation for characterizing the elastic and plastic parameters of ultrafine-grained Al 1050 strips fabricated via accumulative roll bonding process. *Mater. Res. Express* 6 (8), 086542. doi:10.1088/2053-1591/ab18c3

Rani, P., Misra, R. S., and Mehdi, H. (2022). Effect of nano-Sized Al2O3 particles on microstructure and mechanical properties of aluminum matrix composite fabricated by multipass FSW. *Proc. Institution Mech. Eng. Part C J. Mech. Eng. Sci.*, 095440622211108. doi:10.1177/09544062221110822

Sabari, S. S., Malarvizhi, S., and Balasubramanian, V. (2016). Influences of tool traverse speed on tensile properties of air cooled and water cooled friction stir welded AA2519-T87 aluminium alloy joints. *J. Mater. Process. Technol.* 237, 286–300. doi:10.1016/j.jmatprotec.2016.06.015

Sadeghi, B., Sadeghian, B., Taherizadeh, A., Laska, A., Cavaliere, P., and Gopinathan, A. (2022). Effect of porosity on the thermo-mechanical behavior of friction-stir-welded spark-plasma-sintered aluminum matrix composites with bimodal micro-and nano-sized reinforcing Al2O3 particles. *Metals* 12 (10), 1660. doi:10.3390/met12101660

Sahu, S., Mypati, O., Pal, S. K., Shome, M., and Srirangam, P. (2021). Effect of weld parameters on joint quality in friction stir welding of Mg alloy to DP steel dissimilar materials. *CIRP J. Manuf. Sci. Technol.* 35, 502–516. doi:10.1016/j.cirpj.2021.06.012

Salih, O. S., Ou, H., and Sun, W. (2023). Heat generation, plastic deformation and residual stresses in friction stir welding of aluminium alloy. *Int. J. Mech. Sci.* 238, 107827. doi:10.1016/j.ijmecsci.2022.107827

Singh, T., Tiwari, S. K., and Shukla, D. K. (2019). Friction-stir welding of AA6061-T6: the effects of Al2O3 nano-particles addition. *Results Mater.* 1, 100005. doi:10.1016/j.rinma.2019.100005

Singh, T., Tiwari, S. K., and Shukla, D. K. (2020). Effect of nano-sized particles on grain structure and mechanical behavior of friction stir welded Al-nanocomposites. *Proc. Institution Mech. Eng. Part L J. Mater. Des. Appl.* 234 (2), 274–290. doi:10.1177/1464420719885156

Singh, T., Tiwari, S. K., and Shukla, D. K. (2020). Mechanical and microstructural characterization of friction stir welded AA6061-T6 joints reinforced with nano-sized particles. *Mater. Charact.* 159, 110047. doi:10.1016/j.matchar.2019.110047

Srivastava, M., Rathee, S., Siddiquee, A. N., and Maheshwari, S. (2019). Investigation on the effects of silicon carbide and cooling medium during multi-pass FSP of Al-Mg/SiC surface composites. *Silicon* 11, 2149–2157. doi:10.1007/s12633-018-0037-4

Sundaresan, S., and Nageswara Rao, B. (2014). Stress intensity at the initiation of instability by R curve. *Appl. Mech. Mater.* 592, 1160–1164. doi:10.4028/www.scientific.net/amm.592-594.1160

Tayyebi, M., Rahmatabadi, D., Adhami, M., and Hashemi, R. (2019). Influence of ARB technique on the microstructural, mechanical and fracture properties of the multilayered Al1050/Al5052 composite reinforced by SiC particles. *J. Mater. Res. Technol.* 8 (5), 4287–4301. doi:10.1016/j.jmrt.2019.07.039

Teja, P. V. S., and Srinivasan, M. (2024). Friction stir welding of aluminum and its alloy palani Sivaprakasam[1], kolar Deepak[2], durairaj Raja Joseph[3], melaku Desta[1]. *Fricț. Stir Weld. Process. Fundam. Adv.* 25.

Vahdati, M., Moradi, M., and Shamsborhan, M. (2020). Modeling and optimization of the yield strength and tensile strength of Al7075 butt joint produced by FSW and SFSW using RSM and desirability function method. *Trans. Indian Inst. Metals* 73, 2587–2600. doi:10.1007/s12666-020-02075-8

Vamsi, A., Ansari, J., Sundaresan, M. K., Chıtaranjan, P. A. N. Y., Bibin, J. O. H. N., Samridh, A., et al. (2021). *Struct. Des. Test. pouch cells. J. Energy Syst.* 5 (2), 80–91. doi:10.30521/jes.815160

Vimalraj, C., and Kah, P. (2021). Experimental review on friction stir welding of aluminium alloys with nanoparticles. *Metals* 11 (3), 390. doi:10.3390/met11030390

Zhang, Z., Zhang, Z., and Zhang, H. (2014). Numerical investigations of size effects on residual states of friction stir weld. *Proc. Institution Mech. Eng. Part B J. Eng. Manuf.* 228 (4), 572–581. doi:10.1177/0954405413506191

Nomenclature

AA	Aluminum Alloy
Al_2O_3	Aluminum Oxide (Alumina)
ANOVA	Analysis of Variance
AS	Advancing Side
ASTM	American Society for Testing Materials
BM	Base Metal
CCD	Central Composite Design
CNC	Computer Numerical Control
DFSW	Dissimilar Friction Stir Welding
DOE	Design of Experiments
DRX	Dynamic Recrystallization
FSW	Friction Stir Welding
HAZ	Heat Affecting zone
IMC	Inter Metallic Compound
MMC	Metal Matrix Composite
RS	Retreating Side
RSM	Response Surface Methodology
TMAZ	Thermo-Mechanical Affected Zone
TS	Tensile Strength
WNZ	Weld Nugget Zone
YS	Yield Strength